Experimental study of sand deformations during a CPT

A.V. Melnikov & G.G. Boldyrev
Penza State University of Architecture and Construction Engineering, Penza, Russia

ABSTRACT: Cone penetration test (CPT) was simulated in a plane strain test-box and registered by means of particle image velocimetry (PIV) technique. There were measured displacements of sand particles along the cone surface during cone penetration that showed localized shear bands with distinct trends and the deformed zone dimensions.

1 INTRODUCTION

The CPT causes soil deformations that grow from minimal to maximal values, depending on soil strength. Earlier studies showed complicated soil behavior near the cone surface (Allersma, 1987; Chong, 1988; Yu & Mitchell, 1998; Kobayashi & Fukagawa, 2003;Van Nes, 2004; Mo et al. 2012; Salgado 2013).

Allersma (1987) applied optical polarization techniques with photo-elastic elements and discovered a zone of small deformations right below the cone. Chong (1988) showed that several zones rather than one, having different densities, are formed in the course of cone penetration. Later Broere (2001) discovered a shear zone along the cone surface, having used colored horizontal strips in sand. Chong (1988) showed that localized shear strips of different shapes are formed in loose and in dense sand. The zone below the cone, formed by compaction, was caused by low density soil contraction and by compacted soil dilatancy. Kobayashi & Fukagawa (2003) conducted tests in a calibration chamber to investigate the impact of cone tip angle value on the shape of sand deformations during penetration. They concluded that sand deformation behavior is rather insensitive to the value of cone tip angle within the range from 30^o to flat (180^o). In one of his latest studies Salgado (2013) investigated distribution of deformations of dense and loose layers, caused by cone penetration and showed that the width of the deformed zone around the cone is less than 10% of its diameter. General conclusions based on the results by different authors, is that cone penetration destroys soil within a zone adjacent to the cone and to the lower part of the side surface.

Most studies were dedicated to static loading of cone models, and the type of deformations were evaluated by means of soil density measurements (Chong, 1988; Kobayashi & Fukagawa, 2003; Van Nes, 2004; Mo et al. 2012), and to a lesser degree the deformation fields or stresses were measured (Allersma, 1987; Salgado, 2013).

The purpose of this study was to evaluate the type of sand deformations, caused by continuous cone penetration in sand at a fixed rate.

2 TEST TECHNIQUES

Sand deformations, caused by cone model penetration, were measured by means of particle image velocimetry (PIV) technique (White, 2002). The obtained data were processed by the PIVview software code.

The tests were conducted in plain strain configuration, using an automated test set-up (Fig. 1) that included a 720 × 480 × 155 mm test-box and a data-measurement system. The walls of the test-box were made of transparent tampered glass, joined together in one triplex package. In order to resist the soil outthrust the walls were reinforced with metal ribs.

Figure 1. Set-up for plain strain tests

The tested soil was air-dry fine sand. Its physical-mechanical properties are given in Table 1. The soil strength and deformation parameters were determined in plain strain direct shear and 3D compression with standard compression stress path. The sand was poured into the test box from 10 cm height. The density of the sand mass was ρ = 1520 kg/m^3, and its void ratio was e = 0.750. The max void ratio of the sand mass was e = 0.850, and min void ratio was e = 0.563. Max and min void ratio were obtained by the flow rate and the drop height variation.

Table 1. Sand physico-mechanical parameters

Density	Drained friction angle	Elastic modulus	Maximum shear strain at failure
kg/m^3	degrees	MPa	%
1520	35.0	9.7	4.0

The strain for ‘elastic modulus’ in Table 1 was 0.6 %. The probe model was a flat plate (278 × 155 mm) 28 mm thick with 60^o cone angle. The model was made of steel with a roughness ratio 0.44. The model was vertically loaded kinematically at fixed displacement rate with the help of a servo-drive. There was an investigation into loading rate effects that are not covered here. All tests were conducted at 0.42 mm/s probe rate. This rate was a full drive speed. Vertical load was measured by a force sensor, having 0-10 kN range with 0.5 % error. Vertical displacement rate and model position were initiated by stepwise motor at a fixed rate, the number of steps was counted.

The measurement system included a load cell with a data acquisition system, a stepped motor control unit for measuring the number of steps and velocity with RS-232 interface. Loading and penetration processes were automatically controlled by a computer.

PIV was done with a photo-camera (16 Mpix), installed 2.3 m away from the test box and complanar to its transparent wall. The photos were shot automatically each 3 s (i.e. each 1.25 mm of cone penetration) with 1/500 s exposure. Conversion of image pixels coordinates into real physical coordinates with the allowance for image sphericity was achieved with the help of markers, attached on the internal side of the glass. Displacements of soil particles were measured with 0.01 mm accuracy.

3 TEST RESULTS

Test results are shown on Figures 2 to 5. Figure 2 shows the cone model vertical displacements versus total push load. The model loading up to 800 N was followed by intensive sand deformations and penetration resistance growth. Loading up to 800 N caused 129 mm model displacement. Further moderate load increase from 800 to just 900 N resulted in a large displacement increment of 131 mm. Continuous penetration was registered by a sequence of photo snapshots. Figures 3 to 5 show PIV displacements and strain fields at the end of penetration, corresponding to point A on Figure 2.

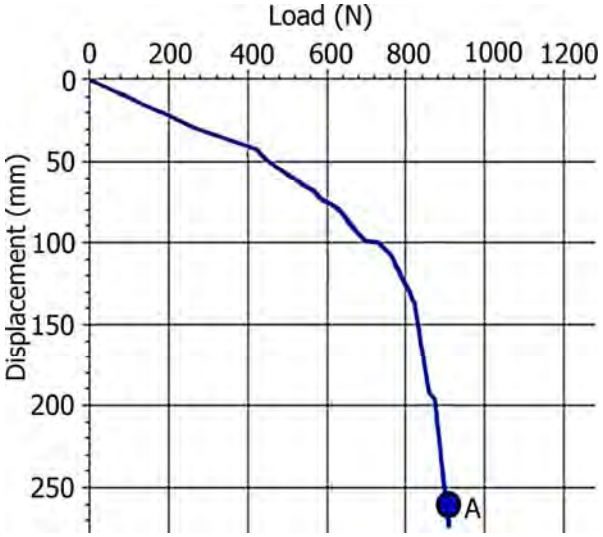

Figure 2. Vertical load versus displacement diagram for model cone in loose sand

Figure 3 shows that the measured deformation zone below the cone was 125 mm (i.e. 2.5 probe diameters), while the measured deformation zone width was maximum 240 mm (i.e. 8.6 probe diameters). Measurement precision was 0.05 mm.

Along with sand movements away from the cone surface there was observed soil movement up toward the surface. Two zones were formed: one of compression (down - D) and the other one of upthrust (upward - E): the first zone moving down while the other one moving up. The boundary between the two zones passed through the cone base of the probe model and can be represented with a direct line (1-2), inclined to the horizon at 35-36^{o} angle. Notably, this angle practically coincides with the angle of soil internal friction equal to 35^{0}.

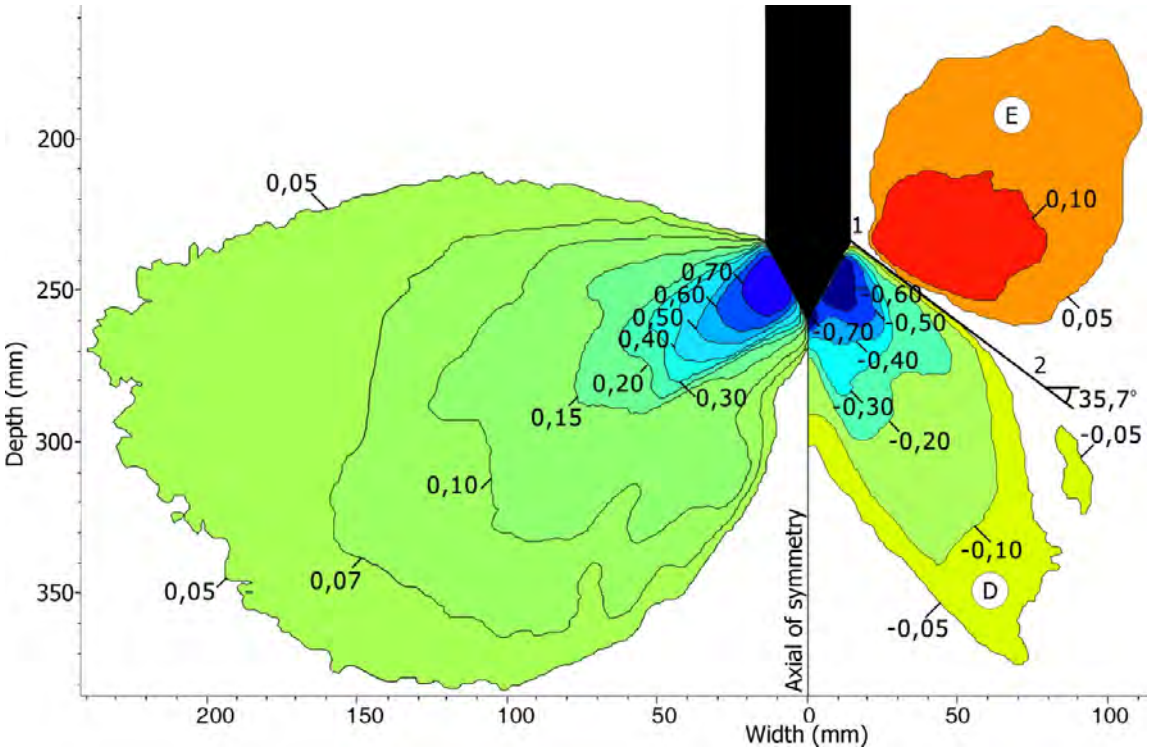

Figure 3. Isolines of horizontal (to the left from the symmetry axis) and vertical (to the right from the symmetry axis) displacements of sand particles.

Figure 4 shows isolines of shear and volume deformations, plotted as per sand particles displacements. Three deformation intensity zones can be delineated in the sand volume, which are separated with straight lines AB and CD (Fig. 4).

1. *Zone of stabilized deformations.* In this zone, located above line AB, stabilized deformations are observed after sand destruction, caused by the probe penetration. This zone can be represented as a cylinder with its base diameter equal to 8.6 diameters of the probe model. Sand within this zone is in limit and super-limit state similar to that below line AB.

2. *Zone of active deformations.* In this zone i.e. below line AB and above line CD, the sand has different strength conditions. As was noted before, 3D compression test yielded ultimate shear deformation of 4 %. Shear deformations values in this zone varied from zero at the zone boundary to 100 % near the cone surface. Also shear strips could be delineated in this zone, in which shear deformation was equal to the limit value. Shear occurred along a series of strips, emerging from the cone tip. As is seen on Figure 4, the family of shear strips looks like “tree roots”.

The test shows there are zones of sub-limit (less than 4 % of shear deformation), limit (4 %) and extra-limit (more than 4 %) condition as to the strength. These phenomena suggests that sand failure is progressive. Initially sand fails at the contact and in the vicinity of the cone side surface, then shear deformations increase by 25 times (100 %), and sand starts simultaneously shearing within narrow strips, emerging from the base and tip of the cone.

3. *Small deformation zone.* Figure 4 shows the active deformation zone that can be limited by CD lines, which emerge just below the cone tip and pass practically parallel to its sides downward. Shear and volume deformations in this zone are small (within the measurement limits) or zero.

Shear deformations are localized in a strip along the model side, whose width does not exceed 1/5 of the probe diameter. A shear strip does not have uniform thickness: closer to the cone base they are wider with shear deformations intensity being greater or equal to the limit one. Maximum values of shear deformations of 4% were observed within 40 mm segment along the probe length (about 1.4 probe diameter) above the cone base. Then they reduced to 0.5 - 2 % to remain practically constant along the probe length.

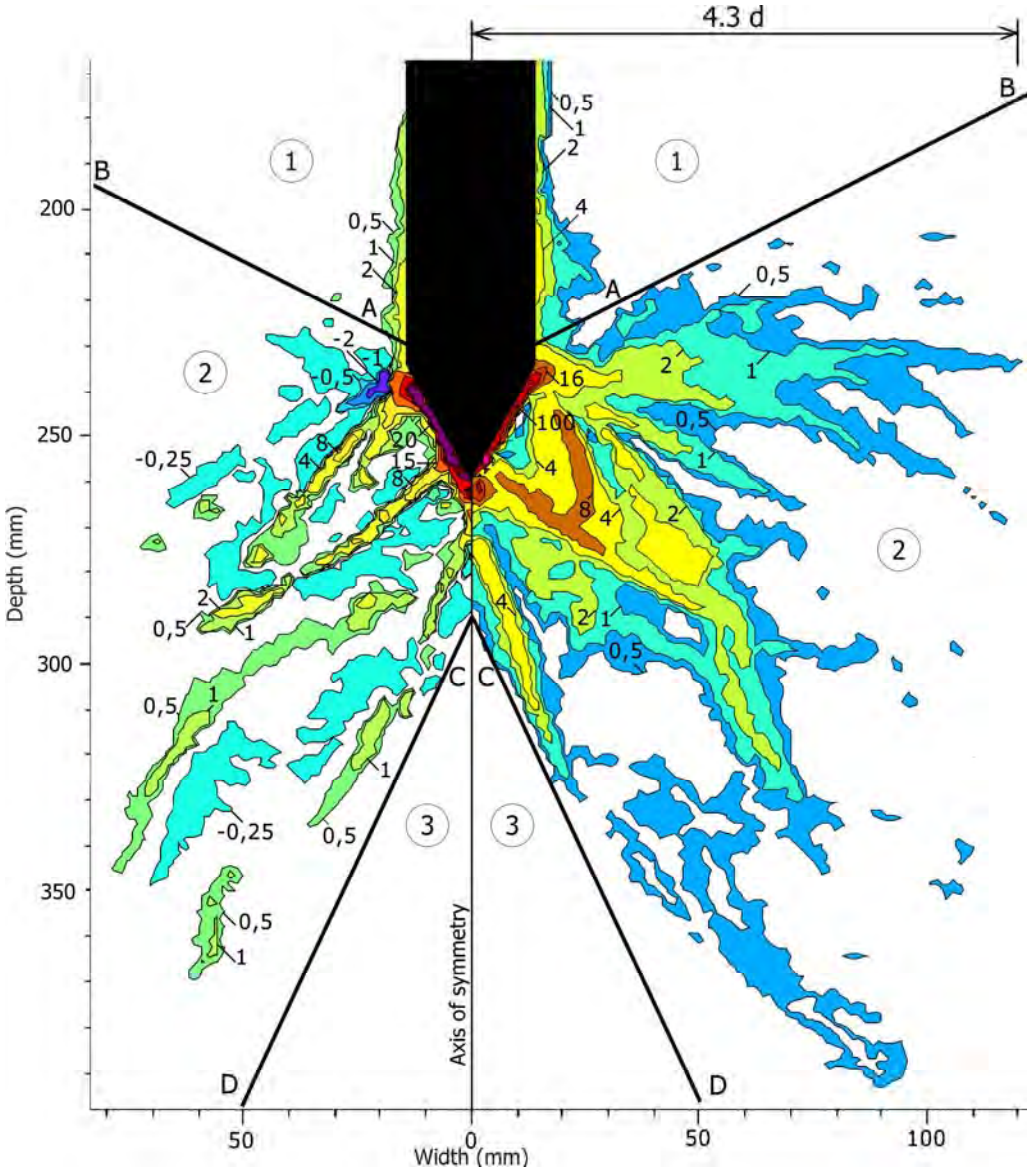

Figure 4. Isolines of compression (to the left of the symmetry axis) and shear deformations (to the right of the symmetry axis: (+) - compression, (-) – expansion, 1 – stabilized deformations zone, 2 – active deformations zone, 3 – deformations absence zone (within the accuracy of measurements)

In spite of low initial sand density (e = 0.75) volume deformations mostly occurred in expansion zones, repeating shear strip shapes. Compression zones were small as compared to expansion ones due to small value of the probe displacement. The volume of sand in the expansion zones was not proportional to the volume in the shear zones. This could be explained by compaction of sand under the cone that resulted in failure of sand not in the whole volume but rather within the strips that intersect the compression zone.

Sand particles were squeezed out of expansion zones that led to extra compression of adjacent zones. The shown deformation images are practically instantaneous snapshots. As different from it, expansion and compression at each fixed point of the sand volume alternated. Maximum deformations reached 20 % and concentrated along the cone oblique surface. Maximum 2 % compression deformations were observed close to the cone tip and a bit below. Along the probe surface at 30 mm distance (one probe diameter) there were observed expansion deformations up to 2 %, reducing at two diameters distance to about 0.5 %.

The test results suggested the following picture of deformations evolution in the sand mass, caused by the probe model penetration, as is shown on Figure 5.

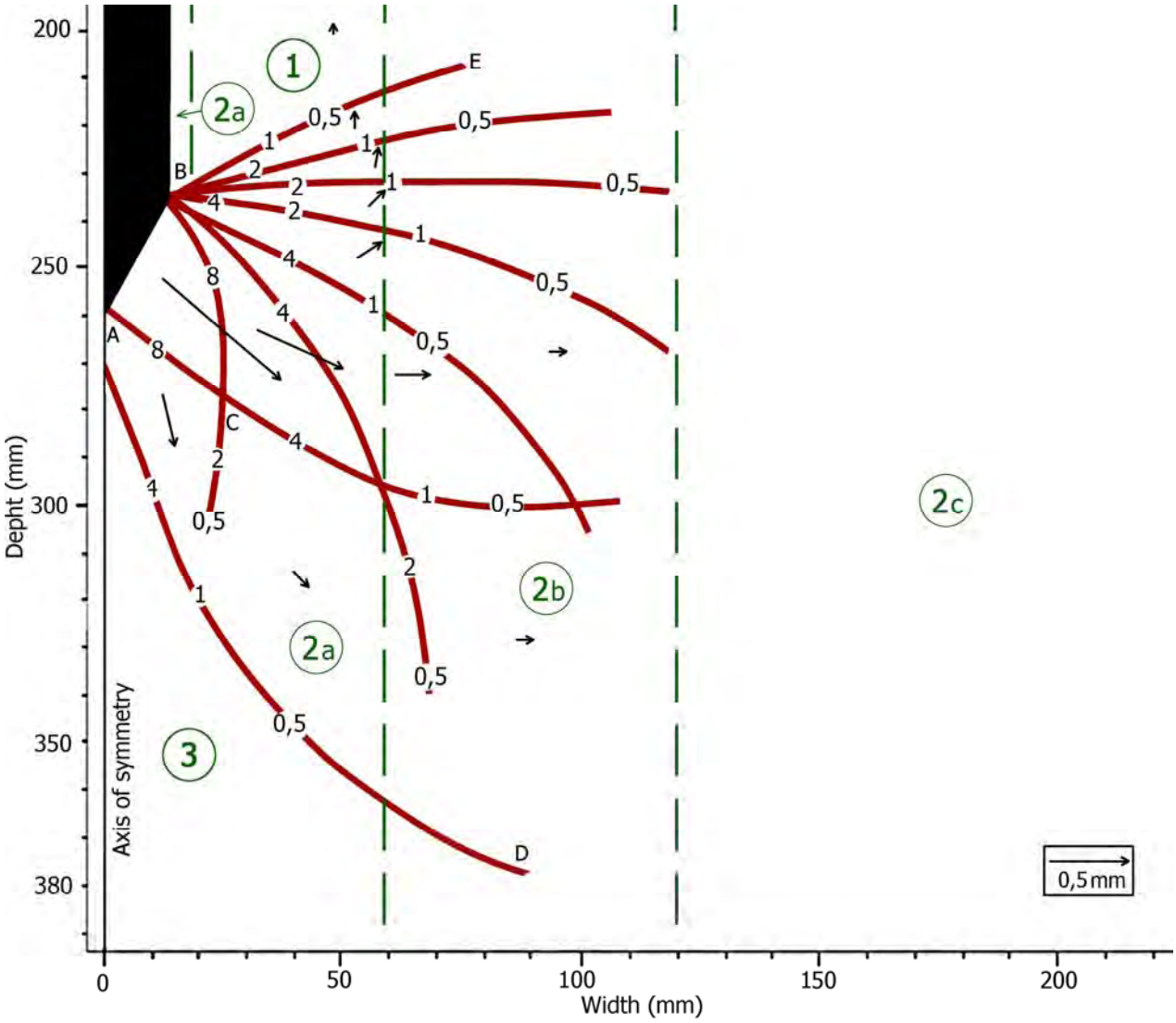

Figure 5. Schematic view of sand deformations around the probe; 1 – stabilized deformations zone; 2a – plastic shear deformations zone; 2b – elastic shear deformations zone; 2c – compaction zone; 3 – small deformations zone.

Figure 5 shows strips, having different shear deformations rates. Their shape was obtained by connecting points in direction of shear deformations reduction from 100 % to 0.5 %. The deformations are less than the limit ones at a certain distance from the cone (about 4 diameters). These strips divided the *zone of active deformations* into two zones (2a, 2b). Vectors on Figure 5 show sand movement directions in each zone while their values correspond to the scale, given at the bottom of the picture on the right. Shear strips form up two families, emerging from the cone tip (point A) and from its base (point B). The wedge-like zone ABC has greatest displacements, and the vector of its displacement is practically normal to the inclined side of cone AB. This zone features maximum shear deformations: 8 % on sides AC and BC and 100 % along cone surface (AB). The plastic deformations zone is comparable with the probe diameter.

In zone 2b shear deformations did not exceed 0.5 % i.e. times 10 less than the ultimate one, therefore, it prompts elastic deformation of the soil.

4 CONCLUSIONS

Based on the limited testing, the following observations can be made:

1. The study and its results demonstrate high effectiveness of the PIV method for assessing sand behavior, caused by probe penetration.

2. The sand mass around the probe can be divided into three zones, having different deformation behavior: a zone of small or zero deformations, a zone of active deformations and a zone of stabilized deformations. The zone of active deformations features localized narrow strips, in which shear deformations exceed sand strength.

3. The study gave rise to an analytical model of sand mass deformations, caused by conic probe penetration. The model has two families of shear (slide) strips, emerging from the cone tip and its base, and divide the soil into zones, in which shear deformations are below limit ones, corresponding to sand strength.

4. Shear deformations are localized within a strip maximum 0.2 probe diameter wide. Shear deformations intensity increases to 100 % close to the cone base.

5. The optimal location of the pore pressure gauge, based on the observed deformation in a loose sand, is behind the friction sleeve, because uniform deformations are observed, as compared with those in the zone around the probe tip, having maximum shear deformations concentration.

5 REFERENCES

Allersma, H.G.B. 1987. Optical analysis of stress and strain in photoelastic particle assemblies. *PhD Thesis*, Delft University of Technology.

Broere W. 2001. Tunnel Face Stability & New CPT Applications *PhD thesis*, Delft University of Technology.

Chong, M. K. 1988. Density changes of sand on cone penetration resistance. *Proc. 1st Int. Symposium on Penetration Testing ISOPT-1, Florida* 2: 707–714.

Kobayashi, T. & Fukagawa, R. 2003. Characterization of deformation process of CPT using X-ray TV imaging technique. *Proc. 3-rd Int. Conf. Deformation Characteristics Geomater., IS-Lyon* 3: 43–47.

Mo, P.Q., Marshall, A.M. & Yu, H.S. 2012 Centrifuge modelling of CPT in layered soils. *Geotechnical and Geophysical Site Characterization 4, ISC-4,* 219-225.

Van Nes, J.H.G. 2004. Application of computerized tomography to investigate strain fields caused by cone penetration in sand. *TA/TG/02-03*, Delft University of Technology.

Ni, Q., Hird C. C. & Guymer I. 2010. Physical modelling of pile penetration in clay using transparent soil and particle image velocimetry. *Geotechnique 60*, No. 2: 121-132.

PIVTEC GmbH. *PIVview User Manual*. Homepage: http://www.pivtec.com.

Salgado, R. 2013. The mechanics of cone penetration: Contributions from experimental and theoretical studies. *Geotechnical and Geophysical Site Characterization* 4: 131-153.

White, D.J. 2002. An investigation into the behaviour of pressed-in piles. *PhD Thesis*, University of Cambridge.

Yu, H.S. & Mitchell J.K. 1998. Analysis of cone resistance: Review of methods. *Journal of geotechnical and geoenvironmental engineering*, 124(2): 140-148.